JACS
JOURNAL OF THE AMERICAN CHEMICAL SOCIETY
Article
pubs.acs.org/JACS

Role of Hydrogen in Graphene Chemical Vapor Deposition Growth on a Copper Surface

Xiuyun Zhang,[†] Lu Wang,[†] John Xin,*[,†] Boris I. Yakobson,*[,‡] and Feng Ding*[,†,‡]

[†]Institute of Textile and Clothing, Hong Kong Polytechnic University, Kowloon, Hong Kong, People's Republic of China
[‡]Department of Mechanical Engineering and Materials Science, Department of Chemistry, and Richard E. Smalley Institute for Nanoscale Science and Technology, Rice University, Houston, Texas 77005, United States

Supporting Information

ABSTRACT: Synthesizing bilayer graphene (BLG), which has a band gap, is an important step in graphene application in microelectronics. Experimentally, it was broadly observed that hydrogen plays a crucial role in graphene chemical vapor deposition (CVD) growth on a copper surface. Here, by using *ab initio* calculations, we have revealed a crucial role of hydrogen in graphene CVD growth, terminating the graphene edges. Our study demonstrates the following. (i) At a low hydrogen pressure, the graphene edges are not passivated by H and thus tend to tightly attach to the catalyst surface. As a consequence, the diffusion of active C species into the area beneath the graphene top layer (GTL) is prohibited, and therefore, single-layer graphene growth is favored. (ii) At a high hydrogen pressure, the graphene edges tend to be terminated by H, and therefore, its detachment from the catalyst surface favors the diffusion of active C species into the area beneath the GTL to form the adlayer graphene below the GTL; as a result, the growth of BLG or few-layer graphene (FLG) is preferred. This insightful understanding reveals a crucial role of H in graphene CVD growth and paves a way for the controllable synthesis of BLG or FLG. Besides, this study also provides a reasonable explanation for the hydrogen pressure-dependent graphene CVD growth behaviors on a Cu surface.

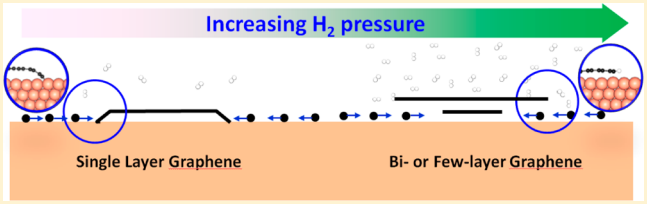

1. INTRODUCTION

Since 2004,[1] graphene has attracted considerable interest because of its prominent mechanical, thermal, conducting, and optical properties and the innumerous potential applications in many fields, such as flexible electronics, spintronics, catalysis, composite materials, energy storage and conversion, etc.[2−7] However, a crucial step with regard to its application in electronics, the synthesis of a high-quality two-dimensional (2D) graphene membrane with a band gap and high carrier mobilities, has never been successfully achieved. Although high-quality and large area single-layer graphene (SLG) has been readily synthesized by chemical vapor deposition (CVD) using copper or other transition metals as a catalyst, it is a gapless semimetal.[8−10] Great effort has been spent to open a band gap in graphene, such as patterning graphene into a narrow ribbon,[3,11,12] chemical doping or physisorption of various molecules,[12,13] applying uniaxial tensile strain,[14] binding the graphene onto a substrates,[14,15] etc. Unfortunately, most of these approaches greatly reduce the mobility of pristine graphene by either disturbing the π electrons or introducing extra boundaries. Another approach to opening a band gap in graphene, the synthesis of bilayer graphene (BLG) or few-layer graphene (FLG) with Bernal (AB) stacking, is more promising because a band gap can be opened by breaking the symmetry between the A and B sublattices and the high mobility can be maintained because little π electron disturbance or new boundaries formed.[16−19]

Experimentally, the synthesis of BLG or FLG with Bernal stacking remains a great challenge. Compared to our understanding of the growth of SLG, which has been extensively studied,[8−10,20−34] our understanding of BLG/FLG growth is still very limited. In a CVD process on a Cu surface, the formation of SLG by the aggregation of active decomposed C species can be easily understood, but the mechanism of formation of the adlayer graphene (ALG) has been debated furiously. Two contradictory models, the wedding cake (WC) model that demonstrates that the ALG is formed above the covered graphene layer on the catalyst surface[35−38] and the inverted wedding cake (IWC) model in which the ALG is formed among the graphene top layer (GTL), the first layer formed on the catalyst surface, and the catalyst surface,[39−41] have been proposed to describe the growth of BLG/FLG on a Cu surface. However, with a detailed characterization, most recent evidence strongly supports the IWC growth model.[39−41]

Although the IWC model has been validated, the detailed growth process of the ALG beneath the GTL at the atomic level has remained a mystery until now. For example, questions like how the active C species (e.g., C_1, CH, CH_2, or CH_3) decomposed on an uncovered Cu surface diffuses between the GTL and the catalyst surface, how a new graphene nucleus is

Received: June 1, 2013
Published: February 5, 2014

   dx.doi.org/10.1021/ja405499x | J. Am. Chem. Soc. 2014, 136, 3040−3047

formed, and how it grows into a large island by adsorbing more active C species remain unanswered.

As reported in many experiments, it is surprising that the hydrogen in the feedstock (normally Ar and CH_4) gas plays a crucial role in the formation of BLG/FLG.[42−45] For example, Yao et al. observed the formation of continuous FLG grown with an increased H_2 flux.[42] Similarly, Liu et al. observed continued BLG growth at a higher H_2/CH_4 ratio and only SLG growth at a low H_2/CH_4 ratio.[45] The experimental data about the formation of SLG and BLG/FLG formed on a Cu surface from more than 10 publications are summarized in Figure 1

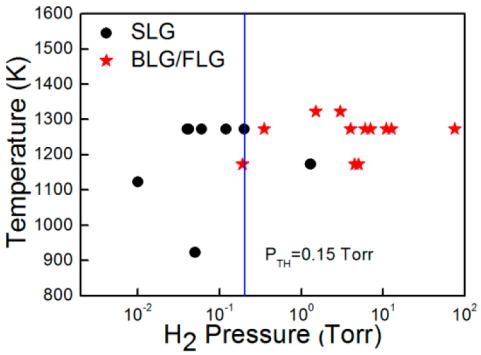

Figure 1. Summary of the experimental data of single-layer graphene (SLG) and bilayer graphene (BLG) or few-layer graphene (FLG) growth on a Cu surface at various temperatures and H_2 pressures (see Table S1 of the SI for details).

and Table S1 of the Supporting Information (SI). It is clearly shown that increasing the H_2 partial pressure results in an abrupt change from the SLG to the BLG/FLG at ∼0.15 Torr. Such a transition is astonishing because two known roles of hydrogen in graphene CVD growth, the etching of graphene and the reduction of the concentration of the active C species on the catalyst surface, do not favor the formation of ALG on a Cu surface. Another well-known effect of hydrogen in graphene CVD growth is its facilitation of the catalytic decomposition of hydrocarbon gases[46] to provide more active carbon species on the free metal surface. However, this does not affect the formation of BLG/FLG. So, why does BLG/FLG growth become favorable at a high hydrogen pressure, and what is the underlying mechanism of hydrogen in graphene CVD growth on a Cu surface?

In this article, to understand the experimental puzzle of the synthesis of BLG/FLG at a high hydrogen pressure and to gain deep insight into the growth mechanism of BLG/FLG on an atomic scale, the formation of graphene edges on a Cu(111) surface as a function of temperature and H_2 pressure, diffusion of active C species on the free and graphene-covered Cu(111) substrate, and their passing through the interface between the free and covered Cu(111) surfaces have been carefully studied by *ab initio* calculations. Our study shows that the C monomer, which is stable and has a low diffusion barrier on a graphene-covered catalyst surface, is the primary type of active C resource for ALG growth. At a low H_2 pressure, the active graphene edge is not terminated by H and therefore bends to the catalyst surface; thus, the active C species can be attached to it easily. In contrast, the inactive hydrogen-passivated graphene edge is favorable at a high H_2 pressure, and thus, the C monomers can pass it freely onto the graphene-covered Cu surface to form the ALG. This study reveals an undetermined role of hydrogen in graphene CVD growth, passivating the active graphene edges and allowing active C monomers to diffuse onto the graphene-covered Cu surface to form the ALG.

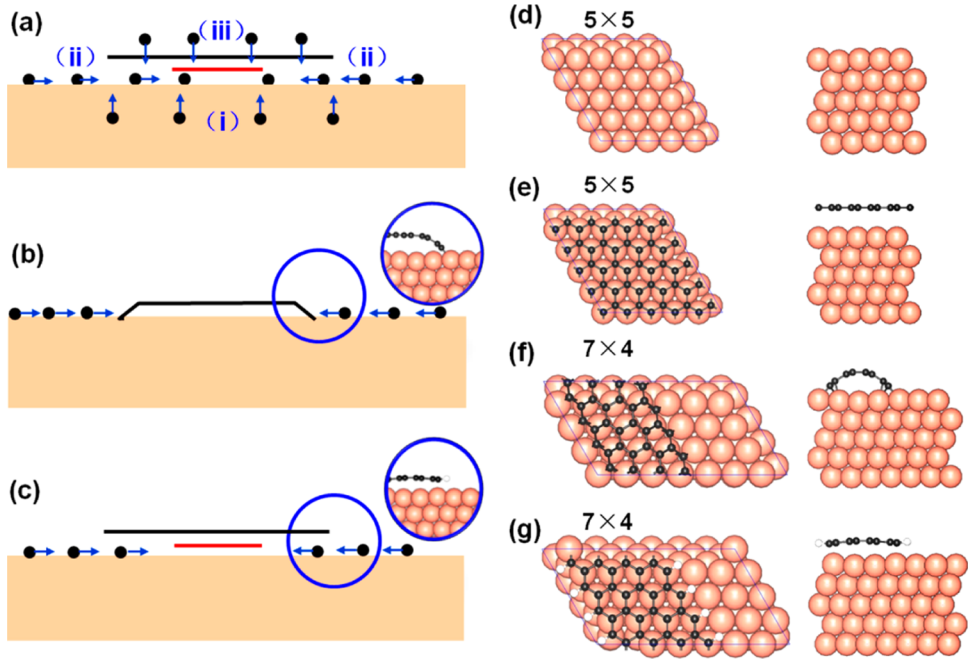

Figure 2. Three potential channels of the active C species to reach the graphene top layer (GTL)-covered catalyst surface for the growth of a graphene adlayer (ALG) (a) and schematic illustration of the graphene (G) growth on a Cu(111) surface with two different types of edges, a metal-passivated edge (b) and a hydrogen-terminated edge (c). (d−g) Top and side views of four different supercells used to study the diffusion of active C species on the catalyst surface with and without GTL (d and e) and the diffusion of the C monomer through the border of metal-passivated (f) and hydrogen-terminated edges (g) of the graphene-covered area.

dx.doi.org/10.1021/ja405499x | *J. Am. Chem. Soc.* 2014, 136, 3040−3047

2. MODELING AND COMPUTATIONAL DETAILS

For the BLG/FLG growth via the IWC model, an active C source beneath the GTL is required. Because the decomposition of the carbon feedstock (i.e., CH_4) mainly occurs on the free catalyst surface unless CH_4 can diffuse freely into the area beneath the GTL (which is impossible as will be shown later), the decomposed active C species (e.g., C_1, C_2, and CH_x, x = 1, 2, or 3) can reach the graphene-covered catalyst surface through three potential channels (Figure 2a): (i) by precipitating from the bulk phase of the catalyst, (ii) by diffusing from the free catalyst surface onto the graphene-covered catalyst surface, and (iii) by reaching the catalyst surface by penetrating the existing graphene.

Among these three channels, channel (iii) requires the graphene to have large defects (like large-fold vacancies to form a hole), and thus, its contribution is very limited for high-quality graphene synthesis. For graphene growth on a Cu surface, channel (i) is also prohibited because of the ultralow solubility of C in Cu. Therefore, we can conclude that an active C species diffusing through the interface between uncovered and covered areas of the catalyst surface is essential for BLG/FLG growth on a Cu surface.

In this study, the Cu(111) surfaces with and without GTL are adopted as an example to explore the formation of BLG/FLG. In CVD growth, depending on the partial pressure of the H_2 in the carrier gas, two types of graphene edges may exist on the metal surface, which are passivated by the metal surface directly at a low H_2 pressure (Figure 2b) or terminated by H atoms (Figure 2c) at a high H_2 pressure. To explore the diffusion of active C species through these two types of the interfaces, two different models, one with the H-terminated graphene edge and another with the metal-passivated graphene edge, are developed (Figure 2f,g).

All calculations are performed within the framework of density functional theory (DFT) as implemented in the Vienna *Ab initio* Simulation Package (VASP).[47,48] The exchange-correlation potentials are treated by the local density approximation (LDA). The interaction between valence electrons and ion cores was described by the projected augmented wave (PAW) method.[49,50] The energy cutoff for the plane wave functions is 400 eV, and a force acting on each atom of <0.02 eV/Å was used as the criterion of convergence in geometrical optimization. The formation of different C species (C_1, C_2, and CH_x, where x = 1, 2, 3, or 4) on a free Cu(111) surface [C@Cu(111), C_2@Cu(111), and CH_x@Cu(111), where x = 1, 2, 3, or 4] and a graphene-covered Cu(111) surface [G@C@Cu(111), G@C_2@Cu(111), and G@CH_x@Cu(111), where x = 1, 2, 3, or 4] is calculated on the basis of the 5 × 5 periodic metal slab model (Figure 2d,e). To explore the diffusion of C atoms through the interface between uncovered and covered Cu(111) surfaces, a 7 × 4 periodic slab model is adopted (Figure 2f,g). All these periodic supercells include five-layer Cu atoms, and the lattice constants of Cu slabs are set the same as those of pristine graphene (2.46 Å), which impose a small strain of ∼3% on the Cu lattice. The lattice sizes of the 5 × 5 and the 7 × 4 models are 12.3 Å × 12.3 Å and 17.22 Å × 9.84 Å, respectively. The Brillion zone is sampled by 2 × 2 × 1 grid meshes for the 5 × 5 slab and 1 × 2 × 1 grid meshes for the 7 × 4 slab by using the Monkhorst−Pack scheme during the calculation. The frequency tests are performed for the two smallest 5 × 5 slabs, G@Cu(111) (Figure 4b) and G@C@Cu(111) (Figure 4g), and two transition states for a single C atom diffusing from the subsurface (Figure 4i,j). Our results show that the optimized structures are indeed local minima with non-negative frequencies, and each transition state is found to have only one imaginary frequency (e.g., −126.11 and −113.48 cm^{-1} for the transition states in panels i and j of Figure 4, respectively). These results showed that the data presented herein are reliable.

For a comparison, the more accurate DFT-D2 method[51] taking into account the van der Waals interaction (VDW) was adopted to explore the formation energy and diffusion of a single C atom and other active C species on both free and graphene-covered Cu (111) surfaces (Figure 4 and Figure S1 of the SI). For the DFT-D2 calculation, the exchange-correlation functional of PBE was performed. Our results showed that the data obtained by LDA calculations agree reasonably well with those obtained by the DFT-D2 calculations. Therefore, considering the time-consuming nature of the DFT-D2 method in comparison with the LDA for the large systems used here, the LDA functional was chosen for most calculations.

3. RESULTS AND DISCUSSION

3.1. Diagram of the Graphene Edge Structure. The diagram of the graphene zigzag edge calculated by the *ab intio* method (see the SI for the details of the calculation) is plotted in Figure 3. It can be seen that the H-terminated edge is

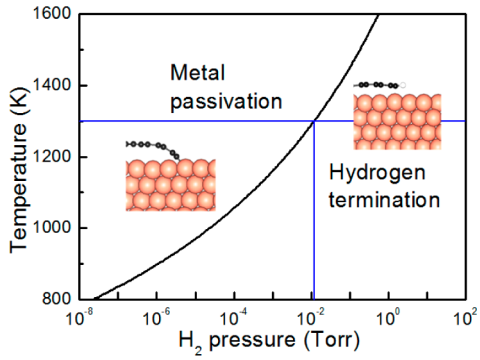

Figure 3. Diagram of graphene zigzag edge formation on the Cu(111) surface at different hydrogen pressures and growth temperatures.

favorable at a low temperature and a high hydrogen pressure, while the metal-passivated edge is preferred at a high temperature and a low hydrogen pressure. This conclusion is consistent with previous studies.[52−55] At a typical graphene CVD growth temperature (T = 1300 K), the transition occurs at a H_2 partial pressure of ∼0.01 Torr. The transition pressure is ∼1 order of magnitude lower than that shown in Figure 1. It should be noted that such a difference implies a formation energy error of $kT \times \ln(10) \sim 0.25$ eV/atom only, and such a small error in the DFT calculation is expected. Therefore, we can say that the theoretically predicted transition pressure is in agreement with the experimentally observed one within an acceptable error.

The agreement between the calculated diagram of graphene edge structures and the experimentally observed transition from SLG to BLG/FLG is not a coincidence. It can be reasonably understood as follows. At a low hydrogen pressure, the graphene edge is attached to the catalyst surface and thus will block the diffusion of active C species from the free area to the graphene-covered area; therefore, there are not enough active C sources beneath the GTL to initiate the nucleation and growth of an adlayer (Figure 2b). On the other hand, once a graphene edge is terminated by H atoms, it becomes less active and will be lifted from the catalyst surface that therefore allows the free transport of C species through the border into the area beneath the GTL to form the ALG and support its growth (Figure 2c).

It is known that Ni is another important catalyst for graphene growth, and graphene growth on Ni showed behavior very different from that on a Cu surface. Diagrams of the graphene zigzag edge on Ni(111) are shown in Figure S2 of the SI. It can be clearly seen that the Ni-passivated graphene edge is much more stable than the Cu-passivated graphene edge, and thus, the transition from the Ni-passivated edge to the H-terminated one occurs at a H_2 pressure of ∼200 Torr at the typical temperature of graphene growth, ∼1200 K. Such a high H_2 pressure is normally not suitable for graphene CVD growth

dx.doi.org/10.1021/ja405499x | J. Am. Chem. Soc. 2014, 136, 3040−3047

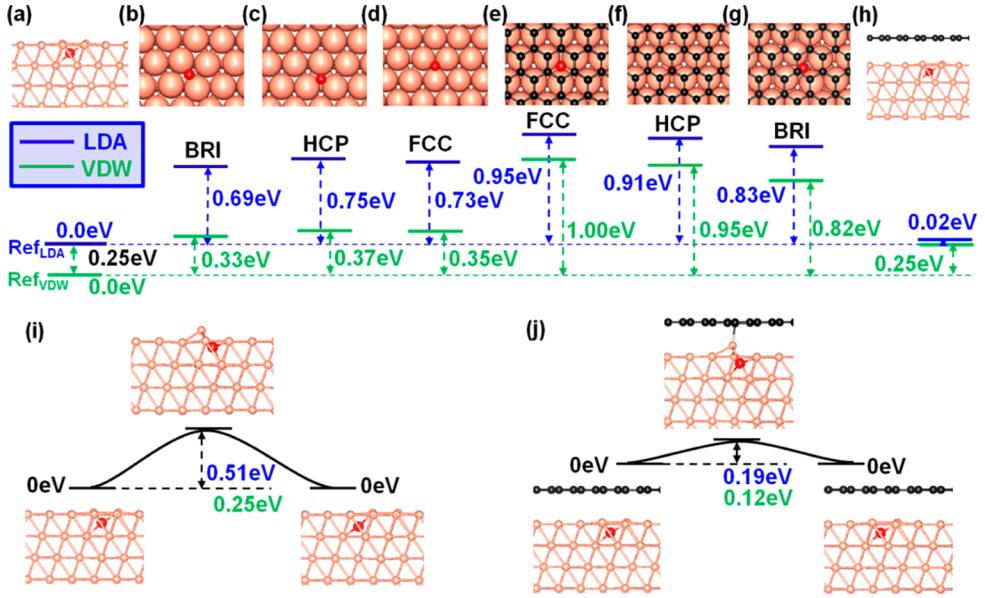

Figure 4. (a–h) Optimized structures and formation energies of the C monomer on different sites of the Cu(111) surface with and without a GTL calculated by both LDA (blue) and VDW DFT-D2 (green) methods. (i and j) Diffusion of the C monomer in the subsurface with and without a GTL, respectively.

because of the etching effect of H_2. This indicates that the hydrogen-terminated graphene edge should dominate the graphene CVD growth on the Ni surface. Therefore, although multilayer graphene is mostly formed on a Ni surface, the hydrogenation of the graphene edge should not play a dominant role for that.

3.2. Active C Species That Are Effective for Graphene Adlayer Growth. During graphene CVD growth, although C monomers (C_1) are expected to be the main form of C precursor for graphene growth on the catalyst surface, other active C species, dimers (C_2) and hydrocarbon radicals like CH_x (x = 1, 2, or 3), are also suspected to be precursors for graphene growth.[8−10,20−23,28,31,34,41,46,56] That is true for the first graphene layer growth, while for adlayer growth beneath the top layer (according to the IWC model), the active species must diffuse into the graphene-covered Cu surface. To give a general understanding of the effective carbon source for adlayer graphene growth, the stabilities of C_1, C_2, and CH_x (x = 1, 2, 3, or 4) on the uncovered and graphene-covered Cu(111) surfaces are calculated (see Figure S1 of the SI). It can be clearly seen that CH_4 beneath the GTL has a significantly large formation energy compared to that on the uncovered Cu(111) surface because of the detachment of the GTL from the catalyst surface. The large formation energy difference, 3.4 eV, will prevent the diffusion of CH_4 through the border between the uncovered and graphene-covered Cu surfaces. The estimated concentration of CH_4 beneath the top layer is only $\exp(-3.4\ \mathrm{eV}/kT) \sim 10^{-15}$ of that on the uncovered Cu surface. This indicates that a CH_4 molecule beneath the GTL is very unstable, and thus, the decomposition of CH_4 on the graphene-covered Cu surface is negligible. Besides the CH_4 molecule, the formation energies of CH_3, CH_2, and CH radicals beneath the top graphene layer are 2.0, 1.6, and 1.2 eV higher, respectively, than those on the uncovered Cu(111) surface. These noticeable energy differences can result in concentration differences of 10^{-9}, 10^{-7}, and 10^{-5}, respectively. Such huge concentration differences imply that the role of these radicals in ALG growth beneath the GTL is also negligible. Like those of CH_4 and those hydrocarbon radicals, the formation energy of C_2 beneath the top layer is also significantly higher than that on the uncovered Cu(111) surface. The energy difference of 1.3 eV implies a huge concentration difference of 10^{-5}.

In contrast, formation of the most stable C monomer [C_1 in the sublayer of the catalyst surface (C_1–I)] is different in that the formation energy difference is only 0.25 eV.[57] The very small energy difference stems from the nearly untouched GTL formation. Differently, the formation of C_1 on the catalyst surface (C_1–II) is less stable than that in the sublayer with a formation energy difference of 0.33 eV. Similarly, beneath a GTL, the formation energy of C_1 on the catalyst surface is increased by 0.5 eV, which is much larger than that in the subsurface. From this analysis, we can conclude that the crucial and active carbon source that can sustainably support ALG growth is the carbon monomer (or C_1) in the sublayer of the catalyst surface. Thus, we will focus on the role of C_1 in the growth of the ALG hereafter.

Either on the uncovered Cu(111) surface or on the graphene-covered surface, there are four potential sites for C_1, namely, the hcp [HCP (Figure 4c,f)], the fcc [FCC (Figure 4d,e)], the bridge site between two metal atoms [BRI (Figure 4b,g)], and the subsurface position (Figure 4a,h). The formation energies of each structure are defined as

$$E_f = E[\mathrm{C@Cu(111)}] - E[\mathrm{Cu(111)}] - E(\mathrm{C}) \quad (1)$$

or

$$E_f = E[\mathrm{G@C@Cu(111)}] - E[\mathrm{G@Cu(111)}] - E(\mathrm{C}) \quad (2)$$

where the E terms represent the energies of C@Cu(111), G@C@Cu(111), the Cu(111) slab, and the C atom from graphene. The optimized structures and calculated formation energies are summarized in Figure 4a–h.

As previously reported,[57] the C atom energetically prefers to sit in the octahedral interstitial site in the subsurface of Cu(111) regardless of whether the surface is covered by GTL. The energy difference in both cases is as low as 0.25 eV,

dx.doi.org/10.1021/ja405499x | J. Am. Chem. Soc. 2014, 136, 3040−3047

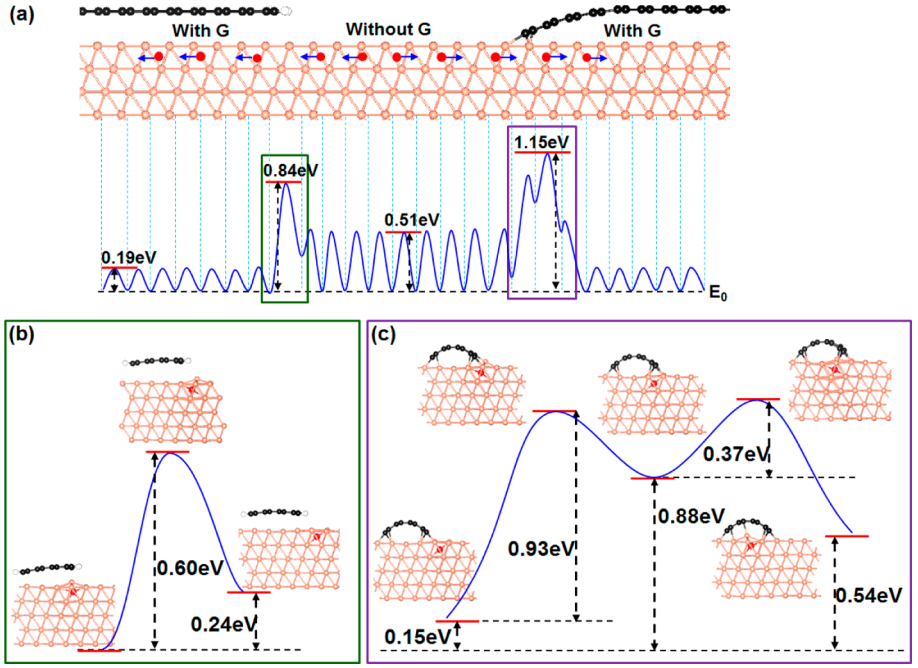

Figure 5. (a) Energy profile of the C monomer diffusing from the free Cu(111) subsurface to the graphene-covered area. The edge of graphene is terminated by hydrogen (left side) or passivated by the Cu(111) surface directly (right side). The details of the diffusion of the C monomer through the hydrogen-terminated graphene edge or metal-passivated graphene edge are shown in panels b and c, respectively.

calculated by the DFT-D2 method (Figure 4a,h). For a C atom sitting on the catalyst surface, three adsorption sites (BRI, HCP, and FCC) are examined, and it is found that all of them have very similar formation energies for both cases. However, the formation energy differences for the cases with and without GTL are significant (0.65, 0.58, and 0.49 eV for FCC, HCP, and BRI sites, respectively).

To show the difference between LDA and DFT-D2 methods, the results calculated by the LDA method are also presented in Figure 4. It can be clearly seen that the order of stabilities calculated by both methods is exactly same but the energy differences between structures with and without GTL are somehow underestimated by the LDA method. For example, the formation energy of the C monomer at the subsurface of the Cu slab with and without GTL calculated by the LDA method is only 0.02 eV, and the differences for C_1 on the Cu surfaces at FCC, HCP, and BRI sites for two cases are only approximately 0.1−0.3 eV.

As the C monomer is crucial C species that supports ALG growth, its mobility is also very important. On the basis of aforementioned discussion, the diffusion of C monomers in the subsurface of the Cu(111) substrate with and without the GTL was explored by the climbing nudged elastic band (cNEB) method.[58] When the C atom migrates between two octagonal sites in the Cu(111) subsurface, a transition state (TS) with the C atom sitting in the center of two octagonal sites is found. For the bare Cu(111) substrate, the activation barrier of migration of a C atom calculated by the LDA method is 0.51 eV (Figure 4i). While the barrier was greatly reduced to 0.19 eV when the catalyst surface was covered by a GTL, such a great reduction in the size of the barrier is surprising because the GTL is far from the Cu(111) surface and is not supposed to affect the behavior of the C monomer in the subsurface. Careful examination of the transition state showed that the Cu atom above the C monomer is pushed upward and forms a bond with the GTL, which stabilizes the new transition state (Figure 4j). This indicates that the C monomer can diffuse more quickly beneath a GTL than on the free Cu surface. The barriers calculated by the DFT-D2 method are also presented in panels i and j of Figure 4. A similar trend is seen, but all the barriers are lower than those calculated by the LDA method. As shown in Figure S4 of the SI, the barriers of C monomer diffusion on the free and covered Cu(111) surface represent an opposite trend in that the barrier of diffusion beneath the GTL (0.18 eV by LDA and 0.13 eV by DFT-D2) is larger than the barrier of diffusion on the bared surface (0.08 eV by both LDA and DFT-D2).

To further verify our results, similar studies were performed for the Ni(111) surface. Very similar tendencies are found for both adsorption and diffusion of C_1 on the surface and in the subsurface (see Figures S3 and S5 of the SI), showing that the reduction of the diffusion barrier beneath the GTL is a general behavior.

3.3. Diffusion of the C Monomer through the Border of Uncovered and Graphene-Covered Cu(111) Surfaces.

As mentioned above, a high hydrogen pressure is essential for the synthesis of the BLG/FLG, and in such a situation, the edge of the GTL is terminated by H atoms. In contrast, at a low hydrogen pressure, the graphene edge would be passivated directly by the metal surface. As suspected previously, the difference of the edge formation is responsible for the growth of the SLG or BLG/FLG. Can the C monomers diffuse freely through the border of the free Cu surface and the H-terminated graphene-covered area? Could the metal-passivated graphene edge effectively stop the migration of the C monomers through the border? To test the proposed hypothesis, the migration of the C monomer through both types of borders was explored (see Figure 5).

As shown in Figure 5a, the metal-passivated zigzag graphene edge bends toward the Cu surface and the distance between the edge atom and the catalyst surface is only ∼0.2 nm. Therefore, the diffusion of the C monomer through such a border is impossible because the graphene edge acts as a fence between

dx.doi.org/10.1021/ja405499x | J. Am. Chem. Soc. 2014, 136, 3040−3047

the free and graphene-covered Cu surfaces. As discussed above, a C monomer tends to be located at an octagonal site of the subsurface, and therefore, its diffusion though the border from the subsurface may not be significantly affected by the metal-passivated graphene edge. For the C monomer diffusing through the H-terminated graphene edge, the calculated barrier is 0.60 eV (details shown in Figure 5b), which is slightly higher than that of its diffusion on the free Cu(111) surface (Figure 4i,j and Figure S4 of the SI). The diffusion of a C monomer through the metal-passivated graphene edge is a bit complicated because of the distortion of the metal lattice caused by the graphene edge attachment (Figure 5c). The overall barrier is 1.15 eV, which is 0.5 eV higher than the barrier for passing through the hydrogen-terminated graphene edge. Certainly, the barrier of 1.15 eV at the temperature of graphene growth ($T \sim 1300$ K) is not sufficient to stop the migration of C monomers through the subsurface to pass the border.

Although the diffusion of the C monomer cannot be effectively stopped by the metal-passivated graphene edge, the active zigzag graphene edge has another role in graphene CVD growth, adsorbing the C monomers that approach it. As shown in Figure 6a, once a C monomer diffuses near a graphene edge,

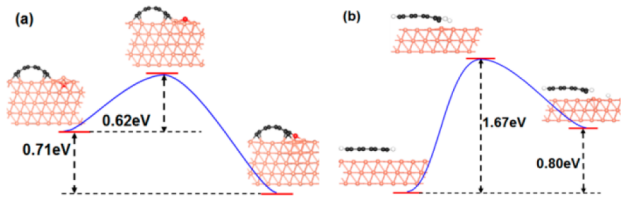

Figure 6. (a) Energy profile of a C monomer being captured by the metal-passivated graphene zigzag edge. (b) Energy profile of a H atom breaking away from the graphene zigzag edge on the Cu(111) surface.

it can diffuse to the catalyst surface and then be adsorbed by the graphene edge. The barrier of such a process is only ~0.62 eV, and it is highly exothermic with a notable energy decrease of 0.71 eV. The direct adsorption of the C monomer in the graphene growth is competitive with respect to C monomer migration through the border. For a C monomer that approaches the graphene edge, it may be captured by the active edge or pass through the border. The rate of the C monomer being captured can be roughly estimated as

$$R_{cap} = \exp(-E_{cap}/kT)/[\exp(-E_{cap}/kT) + \exp(-E_{diff}/kT)] \sim 99.5\% \quad (3)$$

where E_{cap} (0.62 eV) and E_{diff} (1.15 eV) are the activation energies of the C atom being captured by the edge and diffusing through the border, respectively, k is Boltzmann's constant, and T (~1300 K) is a typical temperature of graphene CVD growth. Considering the exothermic reaction of C adsorption, the rate of the C monomer captured at the interface should be even larger than 99%.

Therefore, we conclude that the metal surface-passivated graphene edge acts as an effective drain for adsorbing C monomers. This is in agreement with the growth behavior of graphene on the Cu surface, which was broadly recognized as diffusion-limited growth (DLG) by the fractal-like edge formation of the graphene islands grown at a low hydrogen pressure.[32,59] As the grapene edge is very active for C adsorption, the concentration of the C monomer near the edge would be greatly reduced, and thus, a large concentration gradient would be created on the catalyst surface near the graphene edge. Such a gradient leads to DLG behavior because the graphene growth rate is controlled by the flux of C that diffuses to the edge.

In contrast to the metal-passivated graphene edge, the hydrogen-terminated one is inert in the C monomer or radical adsorption because of the bond-saturated sp^2 edge C atoms. The adsorption of a C monomer by the hydrogen-terminated edge requires the desorption of a H atom from the edge or the breaking of a very stable C−H covalent bond. As shown in Figure 6b, the barrier of breaking a C−H bond on the Cu(111) surface is 1.67 eV and such a process is highly endothermic (energy increases 0.8 eV). Therefore, we can conclude that, near such an edge, the C monomer certainly tends to diffuse into the area beneath the GTL. Such an inert graphene edge also leads to a different graphene growth behavior, attachment-limited growth. In such a case, the growth rate of the graphene is limited by the rate of attachment of the C atom to the edge. Such a growth behavior would result in regular graphene islands (e.g., the regular zigzag edged hexagonal graphene islands[26]) because of the lack of a concentration gradient near the graphene edge.

Relative to the H-terminated graphene edge, the metal surface-passivated graphene edge is much more active because of the weak C−metal interaction. Therefore, a metal-passivated graphene should grow much faster than a H-terminated one. This prediction was recently verified experimentally. As reported by Ryu and co-workers, graphene growth without H_2 gas, which implies that the edge of grapheme is not passivated by H, is ~1 order of magnitude faster than that in traditional thermal CVD experiments.[60]

It is important to note that this discussion also applies to the graphene armchair edge. As shown in Figure S6 of the SI, the subsurface diffusion barrier of the C monomer through the H-terminated graphene armchair edge is only 0.40 eV, which is significantly lower than that of its diffusion through the metal-passivated edges (it is 0.78 eV). The barrier of incorporating one C atom from the subsurface on the edge of the graphene armchair edge is only ~0.55 eV, and it is highly exothermic with a notable energy decrease of 0.74 eV. Therefore, it is clear that the C monomer prefers to be attached to the graphene AC edge instead of passing it to the area beneath the GTL.

To further verify the activity of the two types of graphene edges, *ab initio* molecular dynamics (MD) simulations were performed to explore the growth behavior of the H-terminated and metal-passivated graphene edges on the Cu(111) surface. At the initial stage, all the C atoms are placed in the octagonal sites of the Cu(111) subsurface (Figure 7a,b). By running the MD simulation for 3 ps at 1200 K, we observed attachment of the C atom to the graphene edge for the metal-passivated graphene (Figure 7c) and C diffusing into the area beneath the GTL for the hydrogen-terminated graphene (Figure 7d), indicating that the metal-passivated graphene edge is much more active than the hydrogen-terminated one.

It is important to note that the hydrogen concentration-dependent graphene growth behavior revealed by the analysis described above is in agreement with experimental observations. For example, Vlassiouk et al.[44] showed that graphene islands grown on a copper surface at a low H_2 pressure present the dendrite shape (that is a consequence of DLG) and mostly are SLG and those synthesized at a high hydrogen pressure present a regular hexagonal shape (that is a consequence of ALG) and are mostly BLG or FLG.

dx.doi.org/10.1021/ja405499x | J. Am. Chem. Soc. 2014, 136, 3040−3047

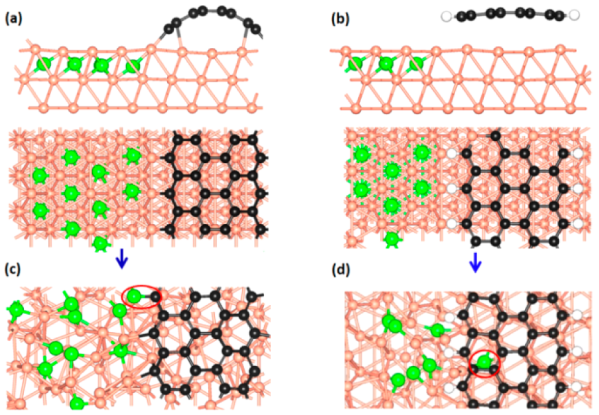

Figure 7. Molecular dynamics simulations of the growth behaviors of the Cu(111) surface-passivated (a → c) and hydrogen-terminated (b → d) graphene edges at 1200 K.

4. CONCLUSION

In summary, the role of hydrogen in the BLG/FLG CVD synthesis on a copper surface is systematically investigated. We found that the C monomer is the primary source for the growth of the adlayer graphene and its diffusion beneath a graphene top layer is significantly faster than that on the free Cu surface. Depending on the pressure of the H_2 gas, the graphene edges can be either directly passivated by the Cu surface (at a low pressure) or terminated by H atoms (at a high pressure). The metal-passivated graphene edge is active for C adsorption, and thus, the C monomers cannot diffuse into the area beneath the graphene top layer to sustain the nucleation and growth of the adlayer graphene. In contrast, the H-terminated graphene edge is not active for C adsorption and thus allows the fast diffusion of C monomers into the area beneath the graphene top layer. Therefore, the metal-passivated graphene edge formed at a low H_2 pressure favors single-layer graphene growth, and the H-terminated graphene edge at a high H_2 pressure favors the growth of bilayer or few-layer graphene. This study successfully explains many debatable experimental puzzles about the role of hydrogen in graphene CVD growth. The method of synthesizing high-quality BLG/FLG graphene by controlling the pressure of H_2 is revealed.

A very recent observation of graphene rings pattern,[61] explained by the subtle potential well near the hydrogenated graphene edge, further emphasizes the key role of hydrogen in switching between single- and few-layer growth, considered here in a comprehensive way.

Here we address the limit of this study that a full understanding of the mechanism of graphene CVD growth requires a precise description of (i) catalyzed feedstock decomposition, (ii) C precursor diffusion on a catalyst surface, (iii) graphene nucleation on a terrace, near a metal step, and on other structural defects, (iv) growth kinetics, (v) healing of defects, and (vi) the formation of a complete graphene layer by the coalescence of graphene islands. Such a full picture is far beyond the scope of this study, and more detailed research is required. In addition, we note that the mechanism proposed in this study can also be applied for the graphene synthesis on other catalysts that have no carbide phase or very low carbon solubility, such as Au, Pt, Pd, Ru, Rh, Ir, etc. On each of these metals, the formation of the second graphene layer requires the carbon supply from channel (ii) (Figure 2). Once the graphene edge is not terminated by the H atoms, the active edge C atoms must be passivated by the catalyst surface, channel (ii) would be closed, and only SLG would be formed on the catalyst surface.

■ ASSOCIATED CONTENT

Supporting Information

Experimental information about the catalysts, carbon feedstock, temperature, pressure, and layer number of graphene from previous studies (Table S1); calculation details of the difference in the Gibbs free energy (ΔG) between H-passivated and free graphene edges; structures and formation energies ofthe C monomer in the subsurface and on the surface and the C dimer and CH_x (x = 1, 2, 3, or 4) on the uncovered and graphene-covered Cu(111) surfaces; diffusion of the C monomer on the bare and graphene-covered Cu(111) and Ni(111) surfaces; diffusion of the C monomer through the hydrogen-terminated armchair graphene edge or metal-passivated edge; diffusion of a C monomer being captured by the metal-passivated graphene armchair edge and a H atom breaking away from the graphene armchair edge on the Cu(111) surface. This material is available free of charge via the Internet at http://pubs.acs.org.

■ AUTHOR INFORMATION

Corresponding Author

feng.ding@polyu.edu.hk; tcxinjh@inet.polyu.edu.hk; biy@rice.edu

Notes

The authors declare no competing financial interest.

■ ACKNOWLEDGMENTS

We acknowledge the support of a Hong Kong GRF research grant (G-YX4Q) and the financial support of PolyU (B-Q26K, B-Q35N) Chinese NSFC grants (No.1110424, 21273189). Work done at Rice was supported by the National Science Foundation grant (CBET-0731246) and in part by the Robert Welch Foundation (C-1590). We thank Dr. Haibo Shu for his help on the diagram of the graphene edge. Computational resources from the Shanghai Supercomputer Center and TIANHE-1 in the Tianjin Supercomputing Center are also acknowledged.

■ REFERENCES

(1) Novoselov, K. S.; Geim, A. K.; Morozov, S. V.; Jiang, D.; Zhang, Y.; Dubonos, S. V.; Grigorieva, I. V.; Firsov, A. A. *Science* **2004**, *306*, 666.
(2) Geim, A. K.; Novoselov, K. S. *Nat. Mater.* **2007**, *6*, 183.
(3) Chen, Z. H.; Lin, Y. M.; Rooks, M. J.; Avouris, P. *Physica E* **2007**, *40*, 228.
(4) Talyzin, A. V.; et al. *ACS Nano* **2011**, *5*, 5132.
(5) Oostinga, J. B.; Heersche, H. B.; Liu, X. L.; Morpurgo, A. F.; Vandersypen, L. M. K. *Nat. Mater.* **2008**, *7*, 151.
(6) Schedin, F.; Geim, A. K.; Morozov, S. V.; Hill, E. W.; Blake, P.; Katsnelson, M. I.; Novoselov, K. S. *Nat. Mater.* **2007**, *6*, 652.
(7) Wu, J. B.; Agrawal, M.; Becerril, H. A.; Bao, Z. N.; Liu, Z. F.; Chen, Y. S.; Peumans, P. *ACS Nano* **2010**, *4*, 43.
(8) Yu, Q. K.; et al. *Nat. Mater.* **2011**, *10*, 443.
(9) Li, X. S.; Magnuson, C. W.; Venugopal, A.; Tromp, R. M.; Hannon, J. B.; Vogel, E. M.; Colombo, L.; Ruoff, R. S. *J. Am. Chem. Soc.* **2011**, *133*, 2816.
(10) Li, X. S.; et al. *Nano Lett.* **2010**, *10*, 4328.
(11) Han, M. Y.; Ozyilmaz, B.; Zhang, Y. B.; Kim, P. *Phys. Rev. Lett.* **2007**, *98*, 206805.
(12) Kan, E. J.; Li, Z. Y.; Yang, J. L.; Hou, J. G. *J. Am. Chem. Soc.* **2008**, *130*, 4224.

(13) Zanella, I.; Guerini, S.; Fagan, S. B.; Mendes, J.; Souza, A. G. *Phys. Rev. B* **2008**, *77*, 073404.
(14) Ni, Z. H.; Yu, T.; Lu, Y. H.; Wang, Y. Y.; Feng, Y. P.; Shen, Z. X. *ACS Nano* **2009**, *3*, 483.
(15) Zhou, S. Y.; Gweon, G. H.; Fedorov, A. V.; First, P. N.; De Heer, W. A.; Lee, D. H.; Guinea, F.; Neto, A. H. C.; Lanzara, A. *Nat. Mater.* **2007**, *6*, 916.
(16) Zhang, Y. B.; Tang, T. T.; Girit, C.; Hao, Z.; Martin, M. C.; Zettl, A.; Crommie, M. F.; Shen, Y. R.; Wang, F. *Nature* **2009**, *459*, 820.
(17) Castro, E. V.; Novoselov, K. S.; Morozov, S. V.; Peres, N. M. R.; Dos Santos, J. M. B. L.; Nilsson, J.; Guinea, F.; Geim, A. K.; Neto, A. H. C. *Phys. Rev. Lett.* **2007**, *99*, 216802.
(18) Ohta, T.; Bostwick, A.; Seyller, T.; Horn, K.; Rotenberg, E. *Science* **2006**, *313*, 951.
(19) Mak, K. F.; Lui, C. H.; Shan, J.; Heinz, T. F. *Phys. Rev. Lett.* **2009**, *102*, 256405.
(20) Marchini, S.; Gunther, S.; Wintterlin, J. *Phys. Rev. B* **2007**, *76*, 075429.
(21) N'Diaye, A. T.; Coraux, J.; Plasa, T. N.; Busse, C.; Michely, T. *New J. Phys.* **2008**, *10*, 043033.
(22) Gao, L.; Guest, J. R.; Guisinger, N. P. *Nano Lett.* **2010**, *10*, 3512−3516.
(23) Ogawa, Y.; Hu, B. S.; Orofeo, C. M.; Tsuji, M.; Ikeda, K.; Mizuno, S.; Hibino, H.; Ago, H. *J. Phys. Chem. Lett.* **2012**, *3*, 219.
(24) Gao, J. F.; Yip, J.; Zhao, J. J.; Yakobson, B. I.; Ding, F. *J. Am. Chem. Soc.* **2011**, *133*, 5009.
(25) Gao, J. F.; Yuan, Q. H.; Hu, H.; Zhao, J. J.; Ding, F. *J. Phys. Chem. C* **2011**, *115*, 17695.
(26) Shu, H. B.; Chen, X. S.; Tao, X. M.; Ding, F. *ACS Nano* **2012**, *6*, 3243.
(27) Gao, J. F.; Zhao, J. J.; Ding, F. *J. Am. Chem. Soc.* **2012**, *134*, 6204.
(28) Zhang, W. H.; Wu, P.; Li, Z. Y.; Yang, J. L. *J. Phys. Chem. C* **2011**, *115*, 17782.
(29) Li, Z. C.; et al. *ACS Nano* **2011**, *5*, 3385.
(30) Wu, P.; Jiang, H. J.; Zhang, W. H.; Li, Z. Y.; Hou, Z. H.; Yang, J. L. *J. Am. Chem. Soc.* **2012**, *134*, 6045.
(31) Li, X. S.; Cai, W. W.; Colombo, L.; Ruoff, R. S. *Nano Lett.* **2009**, *9*, 4268.
(32) Hwang, C.; Yoo, K.; Kim, S. J.; Seo, E. K.; Yu, H.; Biro, L. P. *J. Phys. Chem. C* **2011**, *115*, 22369.
(33) Yakobson, B. I.; Ding, F. *ACS Nano* **2012**, *6*, 5735.
(34) Yu, Q. K.; Lian, J.; Siriponglert, S.; Li, H.; Chen, Y. P.; Pei, S. S. *Appl. Phys. Lett.* **2008**, *93*, 113103.
(35) Kalbac, M.; Frank, O.; Kavan, L. *Carbon* **2012**, *50*, 3682.
(36) Yan, K.; Peng, H. L.; Zhou, Y.; Li, H.; Liu, Z. F. *Nano Lett.* **2011**, *11*, 1106.
(37) Wu, W.; Yu, Q. K.; Peng, P.; Liu, Z. H.; Bao, J. M.; Pei, S. S. *Nanotechnology* **2012**, *23*, 035603.
(38) Robertson, A. W.; Warner, J. H. *Nano Lett.* **2011**, *11*, 1182.
(39) Wu, B.; et al. *Adv. Mater.* **2011**, *23*, 3522.
(40) Nie, S.; Wu, W.; Xing, S. R.; Yu, Q. K.; Bao, J. M.; Pei, S. S.; McCarty, K. F. *New J. Phys.* **2012**, *14*, 093028.
(41) Li, Q. Y.; et al. *Nano Lett.* **2013**, *13*, 486.
(42) Yao, Y. G.; Li, Z.; Lin, Z. Y.; Moon, K. S.; Agar, J.; Wong, C. P. *J. Phys. Chem. C* **2011**, *115*, 5232.
(43) Gao, L. B.; Ren, W. C.; Zhao, J. P.; Ma, L. P.; Chen, Z. P.; Cheng, H. M. *Appl. Phys. Lett.* **2010**, *97*, 183109.
(44) Vlassiouk, I.; Regmi, M.; Fulvio, P. F.; Dai, S.; Datskos, P.; Eres, G.; Smirnov, S. *ACS Nano* **2011**, *5*, 6069.
(45) Liu, L. X.; et al. *ACS Nano* **2012**, *6*, 8241.
(46) Losurdo, M.; Giangregorio, M. M.; Capezzuto, P.; Bruno, G. *Phys. Chem. Chem. Phys.* **2011**, *13*, 20836.
(47) Kresse, G.; Hafner, J. *Phys. Rev. B* **1993**, *48*, 13115.
(48) Kresse, G. F. *J. Comput. Mater. Sci.* **1996**, *6*, 15.
(49) Blochl, P. E. *Phys. Rev. B* **1994**, *50*, 17953.
(50) Kresse, G.; Joubert, D. *Phys. Rev. B* **1999**, *59*, 1758.
(51) Grimme, S. *J. Comput. Chem.* **2006**, *27*, 1787.
(52) Wassmann, T.; Seitsonen, A. P.; Marco Saitta, A.; Lazzeri, M.; Mauri, F. *Phys. Rev. Lett.* **2008**, *101*, 096402.
(53) Zhang, X. W.; et al. *ACS Nano* **2013**, *7*, 198.
(54) Talirz, L.; et al. *J. Am. Chem. Soc.* **2013**, *135*, 2060.
(55) Ziatdinov, M.; Fujii, S.; Kusakabe, K.; Kiguchi, M.; Mori, T.; Enoki, T. *Phys. Rev. B* **2013**, *87*, 115427.
(56) Luo, Z. T.; Kim, S.; Kawamoto, N.; Rappe, A. M.; Johnson, A. T. C. *ACS Nano* **2011**, *5*, 9154.
(57) Riikonen, S.; Krasheninnikov, A. V.; Halonen, L.; Nieminen, R. M. *J. Phys. Chem. C* **2012**, *116*, 5802.
(58) Henkelman, G.; Uberuaga, B. P.; Jonsson, H. *J. Chem. Phys.* **2000**, *113*, 9901.
(59) Fan, L. L.; et al. *Nanotechnology* **2012**, *23*, 115605.
(60) Ryu, J.; et al. *ACS Nano* **2014**, *8*, 950−956.
(61) Yan, Z.; et al. *J. Am. Chem. Soc.* **2013**, *135*, 10755.